Effect of confinement on cross-sectional performance of steel–concrete composite beams with solid and cellular steel sections

Pankaj R. Teware* and Ashish P. Khatri

Department of Applied Mechanics, Visvesvaraya National Institute of Technology, Nagpur 440 010, India

The aim of this study was to compare the moment–curvature (M–ϕ) characteristics of a solid composite section (SCS) and cellular composite section (CCS) of a beam under a sagging moment. The strip method, based on the principles of fundamental mechanics that consider linear strain variation across composite sections, was used to determine M–ϕ. It was first developed for SCS for different parameters, i.e. the grade of concrete, unconfined and confinement strength of concrete, and effective width of a concrete slab, and then extended for CCS. CCS had a 50% depth enhancement over the steel section of SCS. Full interaction between the steel beam and the concrete slab up to the failure of the slab was assumed in the analysis. According to the M–ϕ analysis, CCS enhances the ultimate moment capacity and ultimate curvature for unconfined and confined concrete. Concrete confinement for CCS effectively boosted steel material utilization and resulted in higher curvature ductility before failure. The high concrete strength and wider effective flange width of the slab resulted in high ultimate moment capacity and ultimate curvature for SCS and CCS for unconfined and confined concrete.

Keywords: Composite beams, concrete confinement, moment–curvature characteristics, solid and cellular steel sections.

THE use of composite beams in construction is common due to their advantages. These beams are generally made up of steel–concrete material such that the concrete resists compression generated due to bending. The reduced height from floor to floor due to the shallow depth of the composite beam is one of the advantages of such construction. Often utility ducts are required to pass from one in the other side in the composite beams. Passing these ducts through the web of a steel-rolled section of the composite beams reduces ultimate strength. Higher ultimate strength can be obtained by replacing the rolled steel section (parent section) with a cellular-steel beam having greater depth compared to the parent section. Thus, the use of a cellular composite section (CCS) results in strength enhancement and provision to pass the utility ducts simultaneously.

*For correspondence. (e-mail: pankaj.teware@gmail.com)

Achieving higher ultimate moment (M_u) and ultimate curvature (ϕ_u) is the main prerequisite for composite beam sections. However, the current design codes do not contain any guidelines for proportioning composite beam sections[1,2]. Utilization of composite action has been recognized as an effective way of enhancing structural performance[3]. A good designed composite member can lead to significant savings in terms of section depth, material consumption and overall cost, lower environmental pollution and reduced energy consumption[4]. An effective composite action is formed at a sagging location. This location shows that each material is used to take advantage of its best attributes, making the composite section efficient and economical[5]. It has been proposed that under positive bending, the concrete slab provides buckling resistance to the top flange when subjected to compression[6], and that the ductility of the steel allows for the achievement of high curvature[7]. The behaviour of the composite beam under negative moment is reversed, which results in cracking in the slab and local buckling of the steel profile, influencing the strength and ductility of the beams[8,9]. The ability of the steel flange or web to resist compression depends on its slenderness value, which is represented by its width-to-thickness ratio[10,11]. A simple rigid-plastic analysis of the section was carried out, which showed that the positive moment capacity of a member could be increased by as much as 120% over the plain steel beam through composite action[12]. Analytical and experimental work was carried out to predict the ultimate strength and ensure the ductility of composite girders constructed using 250, 345 or 485 MPa grades steel[13]. This study showed that a higher grade of steel enhanced the moment capacity but resulted in limited ductility of the composite section[13]. A study reported the failure of a composite beam with high-strength steel or concrete compared to those with normal-strength steel and concrete[14]. A method was presented for the ultimate strength analysis of composite beams with unreinforced rectangular web openings[15]. It was observed that the strength of a composite beam decreases with an increase in opening length and height. The location of the concentric web holes also plays an important role in resisting the vertical load of the composite beam. An experimental study examined the effect of concrete and steel strength, and concrete slab thickness on both buckling and

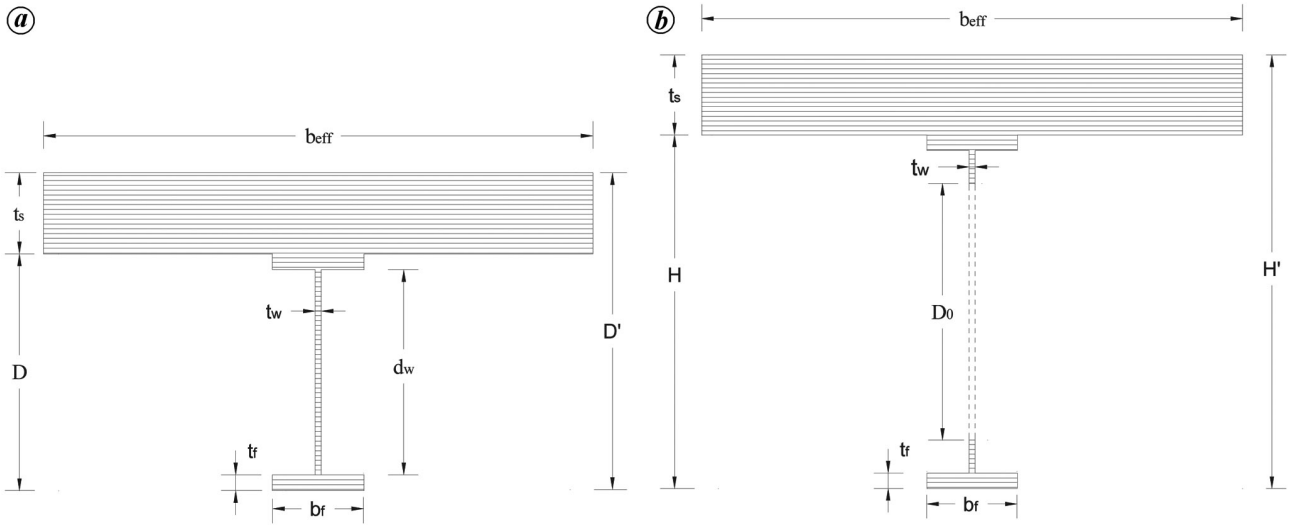

Figure 1. Typical cross-section of composite beams. (***a***) Solid composite section (SCS) and (***b***) cellular composite section (CCS).

the overall structural behaviour of composite beams under vertical load[3]. Results proposed a 25% increment in the ultimate load-carrying capacity of the composite castellated beam if web opening was provided after the negative moment region. To examine the effect of castellation (hexagonal opening) on moment capacity and mid-span deflection of the composite beam, different castellation ratios were considered[16]. The results showed a reduction in mid-span deflection and improvement in moment capacity with an increased castellation ratio[16]. Ferreira *et al.*[17] provided more details about the cellular composite beams. Concrete confinement also plays an important role in increasing the compression resistance of concrete according to the stress–strain equation[18,19]. Ductility is a linear function of lateral confining pressure[20]. The confinement can be achieved by varying the spacing of the stirrups. The ultimate strength capacity and ductility of concrete beams increase as the stirrup spacing decreases. Stirrups that enclose concrete in the compression zone are more efficient than those that run around the entire beam cross-section[21,22]. To achieve satisfactory flexural strength and ductility, it was proposed to stirrups be effectively placed in the bending zone[23,24].

Recent studies have concentrated more on the behaviour of web posts of the cellular composite beams, high-strength material and buckling behaviour. It is still necessary to study how the composite beam cross-section performs under the influence of confined or unconfined strength of concrete and structural steel with the cellular opening provided in the web. The present study particularly focused on exploring this behaviour in the form of the moment–curvature (M–ϕ) relationship of CCS and SCS. A cellular beam section is defined as a steel beam with repeating concentric circular web openings. It is assumed to be made up of its parent rolled parallel flange section with a depth enhancement of 50%. It can be made from hot-rolled profiles by double-cutting and rewelding processes. Figure 1 *a* and *b* show the typical cross-section of SCS and CCS respectively. For developing an M–Φ relationship, full interaction without any slip between steel and concrete is assumed. The M–Φ characteristic of the composite beam was first developed for SCS and later for CCS.

Algorithm of the developed program

The M–Φ analysis was performed based on the structural principles of mechanics. Figure 2 is a flowchart of the developed program for M–Φ analysis, including iterative calculations. The variation of strain across the cross-section of SCS and CCS was considered linear (Figure 3 *a* and *b*). The analysis was first carried out for SCS for unconfined and confined concrete. The same procedure was modified and used for CCS by neglecting the contribution of web opening and assuming linear strain variation across the depth of the section.

The effectiveness of different cross-sections used for analysis was expressed in terms of the percentage utilization of steel and concrete respectively. Percentage utilization of steel is the ratio of total tensile and compressive forces resisted by the steel section at the failure stage to its capacity when all fibres are yielded. Similarly, the percentage utilization of concrete is the ratio of the area of concrete under compression at the failure stage to the total area of concrete. These utilization ratios give an idea to effectively proportionate the cross-section area of steel and concrete for maximum use, and make the section economical and efficient.

Reliability of the developed program

Numerical simulation for CCS beams was done before the start of the parametric analysis. The finite element model

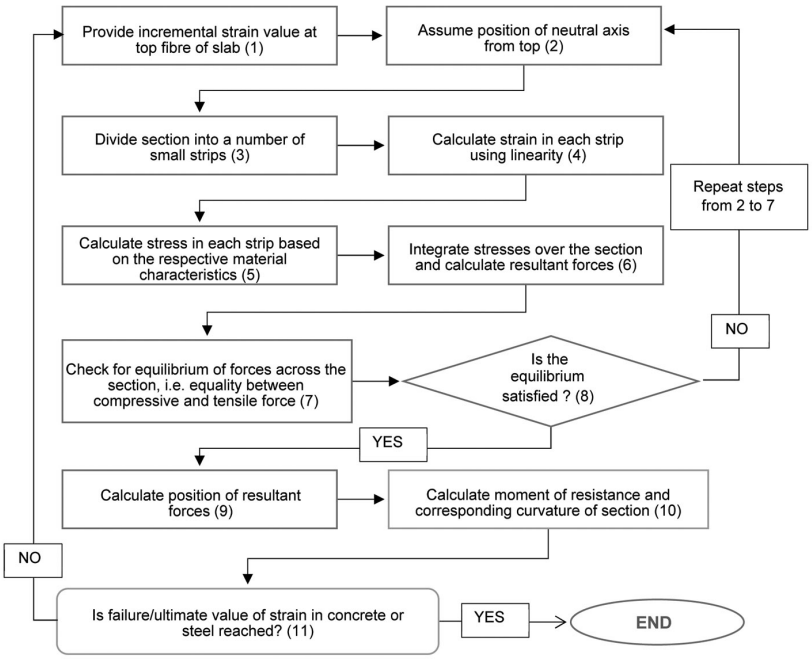

Figure 2. Flowchart of the developed program for moment–curvature analysis.

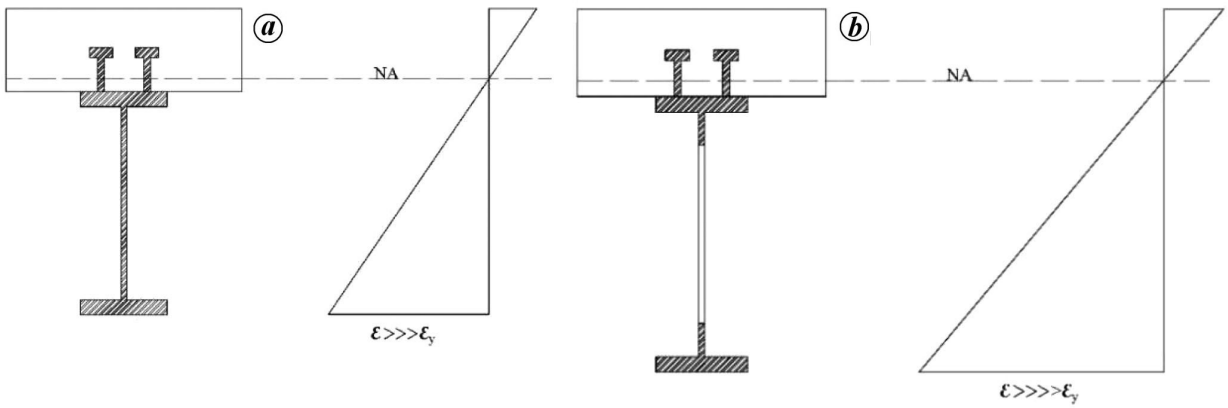

Figure 3. Strain variation in composite cross-sections at the intermediate stage. (***a***) SCS and (***b***) CCS.

(FEM) for the developed program was generated using the same model setup as the numerical simulation, which was successful. The results of the developed program and FEM can be used for parametric analysis once they have been verified.

Numerical validation

The findings of cellular composite beams were used to validate the present FEM through deflection response (d_{FEM})[25]. The present FEM of the beam is a supported cellular composite beam subjected to a concentrated load at mid-span (Figure 4). The shear connectors embedded in solid concrete slabs are used. Four-noded shell elements and four-noded multi-layered shell elements are used for the steel beam and concrete slab, while two-noded beam elements are used for connectors. The steel, concrete and studs are characterized by linear elastic behaviour. The deflection response of the present FEM was validated with that reported in the literature[25], which incorporated the additional deflection due to cellularity, and with the equation proposed for cellular composite beams[25–27]. Compared to the present FEM, the deflection predicted by the equation was consistent (Table 1).

Validation of the developed program

To validate the developed program, solid 3D FEMs of laterally restrained composite beams with 600 mm effective width of the slab (b_{eff}), 200 mm slab thickness and 6000 mm

supported span were developed for different SCS and CCS (Figure 5). These FEMs were then subjected to uniform moment loading conditions to avoid any shear deformation in the beams. The parent NPB sections had a depth (H) upsurge of 50% ($H = 1.5D$) over their original depth (D)[28], and the diameter of the provided web opening (d_0) was 67% of their enhanced depth ($d_0 = 0.67H$). Figures 6 and 7 show the response of composite beams in terms of stress and strain. Figure 8 shows the M–φ relationship. The M–φ behaviour of composite beams as determined by present FEM and the developed program shows good agreement for all the considered beams (Figure 8). All the behaviour shown is captured at the maximum allowable strain level of 0.0035 of concrete, which is also the threshold for failure for composite beams. Using this validated FEM set-up, the results of M–φ of SCS and CCS, proposed using the developed program, were thus verified.

Parametric details

The aforementioned algorithm was used for analysing the M–Φ relationship of composite beams considering different parameters, i.e. the strength of unconfined concrete, degree of confinement to the concrete and effective flange width of the slab.

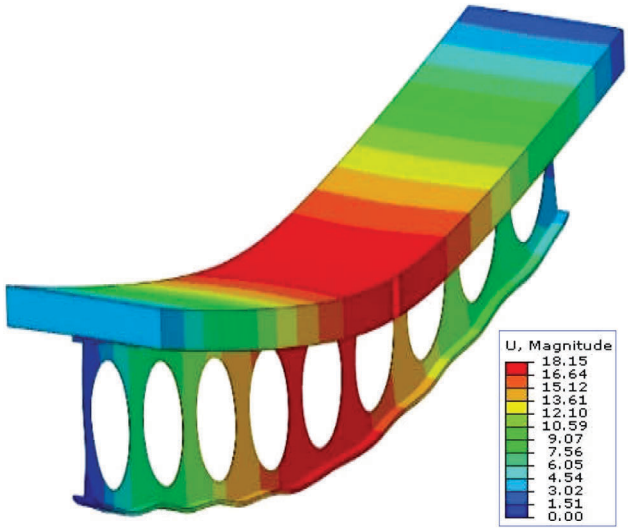

Figure 4. The present finite element model (FEM) of cellular composite beams.

Table 1. Total deflection of cellular composite section (CCS) beam

Specimen	Deflection (mm)	d_{FEM}/d_i
d_{FEM}	18.15	1.00
d_1 (ref. 25)	18.00	0.99
d_2 (ref. 26)	18.00	0.99
d_3 (ref. 27)	16.70	0.92

Geometric characteristics

Hot rolled parallel flange NPB 350 × 250 × 79.18 section was considered as the parent steel section for the composite beam[28]. The cellular beam used was obtained from the parent section and had a 50% depth enhancement without any increase in the total weight of the beam compared to the parent section. To avoid the practical challenges of installing confining reinforcement to concrete, a minimum 200 mm depth of concrete slab was considered. Table 2 shows the parameters considered along with their variation for analysis. The strength and ductility of the confined concrete depend on the arching action between the longitudinal bars and between transverse stirrups and links. Three different grades of concrete were considered to determine the effect of concrete grade on confinement (Table 2)[29]. The assumed reinforcement for providing confinement effect to the concrete slab is as per Table 3.

The steel and concrete grades, as listed in Table 2, were considered for analysis to examine their effect on composite beams. The stress–strain curve for concrete was developed based on its characteristic material strength[29]. The material characteristics used for the study did not include the corresponding material safety factors. However, a size and shape correction factor of 0.85 was applied to the concrete used in the present study. The tensile strength of concrete was also neglected. Without considering the material safety factor, the bi-linearised material stress–strain characteristics were used for structural steel beams, both in tension and compression.

Structural steel: Steel E250 grade was considered for M–Φ analysis[30]. The bi-linear stress–strain curve shown in Figure 9 was used without considering the effect of strain hardening. Failure of the composite section is bound to occur when strain at the top fibre of the concrete slab reaches its ultimate strain value (ε_u), i.e. 0.0035. The corresponding value of ultimate strain in steel at the ultimate stage never reaches up to the strain hardening value, and hence strain hardening effect in steel was neglected during analysis. Furthermore, it was assumed that the stress–strain characteristics of steel are the same in both the compression and tension zones.

Unconfined concrete: In the present study, idealized stress–strain properties of unconfined concrete were considered for M25, M35 and M50 grades of concrete (Figure 10). The maximum flexural stress in concrete was considered $0.85f'c$ (where $f'c = 0.8 \times f_{ck}$, f_{ck} is the characteristic strength of concrete cube)[29]. The obtained unconfined compressive strength for M25, M35 and M50 grades of concrete was 16.75, 23.45 and 33.50 MPa respectively. The maximum stress in concrete was at a strain value of 0.002, after which the stress was constant up to the ultimate strain of concrete. Figure 10 shows the behaviour of concrete at the yield and ultimate point for all the considered grades.

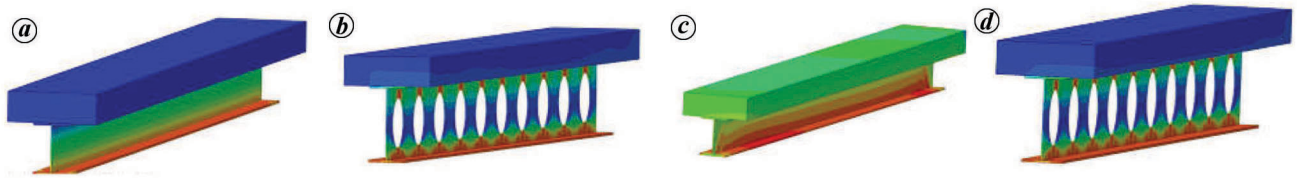

Figure 5. FEM of composite beams. ***a***, SCS beam, unconfinement; ***b***, CCS beam, unconfinement; ***c***, SCS beam, confinement; ***d***, CCS beam, confinement.

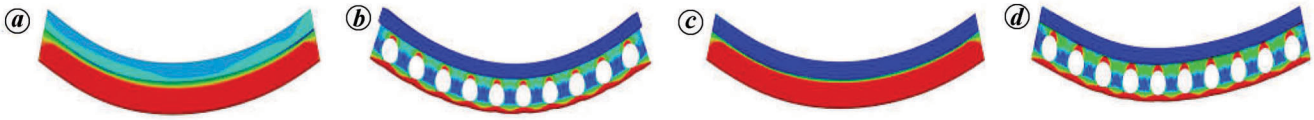

Figure 6. Stress variation in composite beams. ***a***, SCS beam, unconfinement; ***b***, CCS beam, unconfinement; ***c***, SCS beam, confinement; ***d***, CCS beam, confinement.

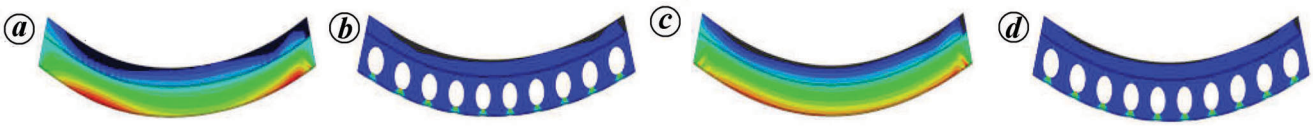

Figure 7. Strain variation in composite beams. ***a***, SCS beam, unconfinement; ***b***, CCS beam, unconfinement; ***c***, SCS beam, confinement; ***d***, CCS beam, confinement.

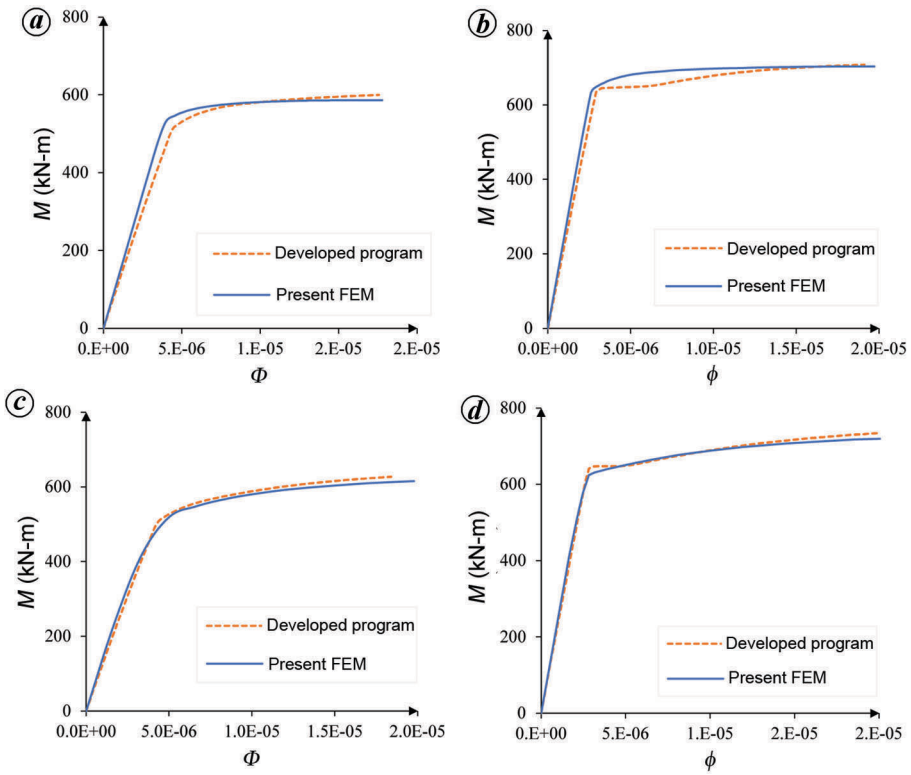

Figure 8. Moment–curvature behaviour of composite beams. ***a***, SCS beam, unconfined; ***b***, CCS beam, unconfined; ***c***, SCS beam, confined; ***d***, CCS beam, confined.

Confined concrete: The energy-balanced concept was used to predict the longitudinal compressive strain in concrete corresponding to the first fracture of the transverse reinforcement by equating the strain energy capacity of the transverse reinforcement to the strain energy stored in concrete as a result of the confinement[19]. In the present study,

Table 2. Parameters considered for solid composite section (SCS) and cellular composite section (CCS)

Solid steel section	Cellular steel section	Slab geometry (mm)		Material grade (MPa)	
Details of NPB 350 × 250 × 79.18 (mm)		b_{eff}	t_s	Concrete	Steel
Depth (D) = 340					
Width of flange (b_f) = 250	Enhanced depth (H) = 1.5 × D	600	200	M25, M35 and M50	E250
Thickness of flange (t_f) = 14	Diameter of web opening (D_o) = 0.67 × H	800			
Depth of web (d_w) = 312	d_{wp} = 482 mm	1000			
Thickness of web (t_w) = 9					

t_s, Thickness of slab; d_{wp}, Depth of web post.

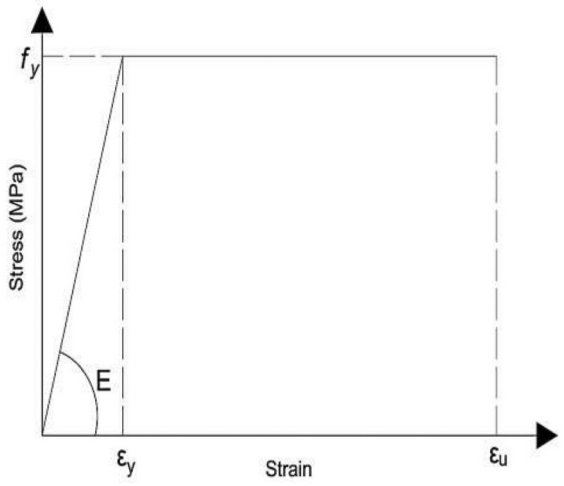

Figure 9. Bi-linear stress–strain curve of steel for both tension and compression.

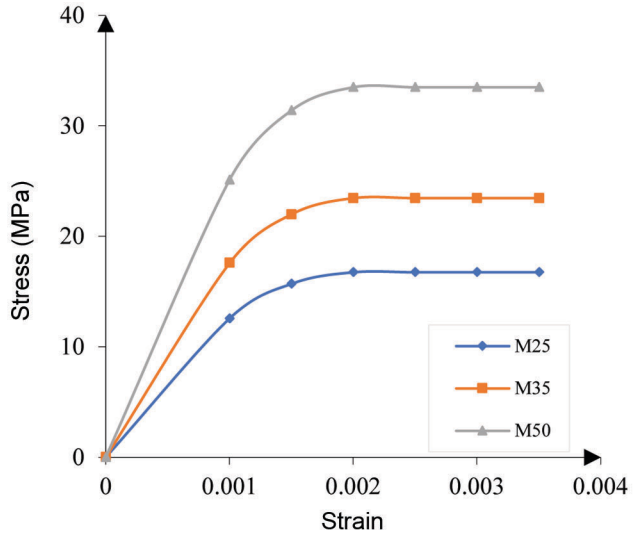

Figure 10. Idealized stress–strain curve of concrete in compression.

to find the confined strength of concrete, a stress–strain model was used[19]. The model included strength degradation characteristics after attaining the maximum confining strength and increased strain value. Confinement of concrete by suitable arrangement of transverse reinforcement resulted in a slight increase in the flexural strength and a significant improvement in strain ductility of compressed concrete. The effectiveness of transverse reinforcement depends on the size of the confining core, which depends on the spacing between the longitudinal reinforcement. For this, we considered different assumed longitudinal reinforcement details and the corresponding transverse reinforcement thereof for different flange widths of the concrete slab (Figure 11). An earlier proposed equation was used to generate the confined stress–strain curve for the considered grades of concrete[19]. The basic expression representing the proposed stress–strain relation is presented below.

For a monotonic loading, the longitudinal compressive stress f_c is given by

$$f_c = \frac{f'_{cc} xr}{r - 1 + x^r}, \tag{1}$$

$$x = \frac{\varepsilon_c}{\varepsilon_{cc}}, \tag{2}$$

where x is the ratio of compressive strain in concrete to the strain at peak stress and ε_c is the longitudinal compressive concrete strain.

$$\varepsilon_{cc} = \varepsilon_{co}\left[1 + 5\left(\frac{f'_{cc}}{f'_{co}} - 1\right)\right], \tag{3}$$

where f'_{co} and ε_{co} are the unconfined concrete strength and the corresponding strain (ε_{co} = 0.002 is used) respectively.

$$r = \frac{E_c}{E_c - E_{sec}}, \tag{4}$$

$$E_c = 5000\sqrt{f'_{co}}, \tag{5}$$

where E_c is the tangent modulus of elasticity of concrete and E_{sec} is the tangent modulus for confined concrete

$$E_{sec} = \frac{f'_{cc}}{\varepsilon_{cc}}, \tag{6}$$

where f'_{cc} is the compressive strength of confined concrete.

Table 3. Details of reinforcement in the concrete slab of the composite section

b_{eff} (mm)	Assumed reinforcement on each face along the beam	Confining reinforcement of 8 mm diameter @ 175 mm c/c
600	4 bar 12 mm in diameter	Two numbers of two-legged stirrups
800	5 bar 12 mm in diameter	Two numbers of two-legged stirrups + two links
1000	7 bar 12 mm in diameter	Three numbers of two-legged stirrups + three links

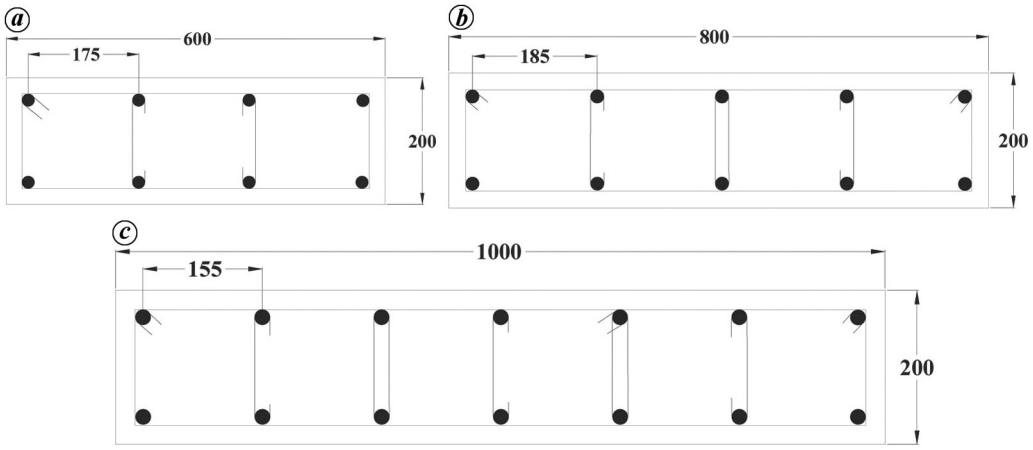

Figure 11. Arrangement of reinforcement in the concrete slab for a different b_{eff} values. ***a***, b_{eff} = 600 mm; ***b***, b_{eff} = 800 mm; ***c***, b_{eff} = 1000 mm.

$$f'_{cc} = f'_{co}\left(-1.254 + 2.254\sqrt{1+\frac{7.94f'_l}{f'_{co}}} - 2\frac{f'_l}{f'_{co}}\right), \quad (7)$$

where f_l is the effective lateral confining stress on concrete. Using eqs (1)–(7), the confined compressive stress–strain characteristics for different grades of concrete and different effective widths were obtained (Figure 12).

From Figure 12 *a–c*, it is clear that a concrete slab with an effective flange width (b_{eff}) of 1000 mm with 155 mm centre-to-centre longitudinal bar spacing shows higher confined strength and failure strain than the others. This is due to the accessibility of high confining reinforcement available for the core concrete section. The strength and ductility of the section are increased, as they are directly related to the amount of confinement available. Likewise, a lower grade of concrete has a higher percentage increase in strength and ultimate strain than a higher grade of concrete.

Behaviour of composite cross-section

All the possible combinations of the parameters mentioned in Table 2 were used to determine the cross-sectional behaviour of SCS and CCS through the M–φ relationship. The analysis was divided into two stages based on the strain value of the cross-section, i.e. elastic stage and inelastic stage. In the elastic stage, linear stress–strain behaviour was adopted for analysis, while in the inelastic stage, the yielding started from the extreme fibre towards the neutral axis (NA). The analysis was terminated when the concrete material reached its ultimate failure strain. Analysis results were compared based on M_u, φ_u, and percentage utilization of steel and concrete material of the cross-section. All the composite sections showed initiation of yielding strain in the bottom flange of steel before attaining the 0.002 strain level at the top fibre of concrete. For plotting the analysis results, a non-dimensional ratio between the moment capacity of section (M) and moment capacity at the yielding of section (M_y), and similarly, for the curvature of section (ϕ/ϕ_y) was determined.

Effect of unconfined and confined strength of concrete

The composite section was analysed for the effect of unconfined and confined strength of different grades of concrete on SCS and CCS (Table 4). From Table 4, it can be observed that M_u and φ_u are improved for CCS compared to SCS. The composite beam with CCS exhibited improvements in M_u and φ_u of 18% and 12% respectively, over SCS for a 600 mm wide concrete slab for unconfined M25-grade concrete. For higher grades of concrete, i.e. M50, improvement in M_u and φ_u was 10% and 17% respectively. This exemplifies how more ductile sections can be attained with a relatively low improvement with higher-grade concrete.

Table 4 clearly shows that CCS exhibits better ductility and moment resistance capacity when taking into account the confined strength of concrete for cross-sectional performance. CCS exhibits a 17% and 5% improvement in M_u and φ_u of the section respectively, in comparison to SCS for a 600 mm wide concrete slab when confinement

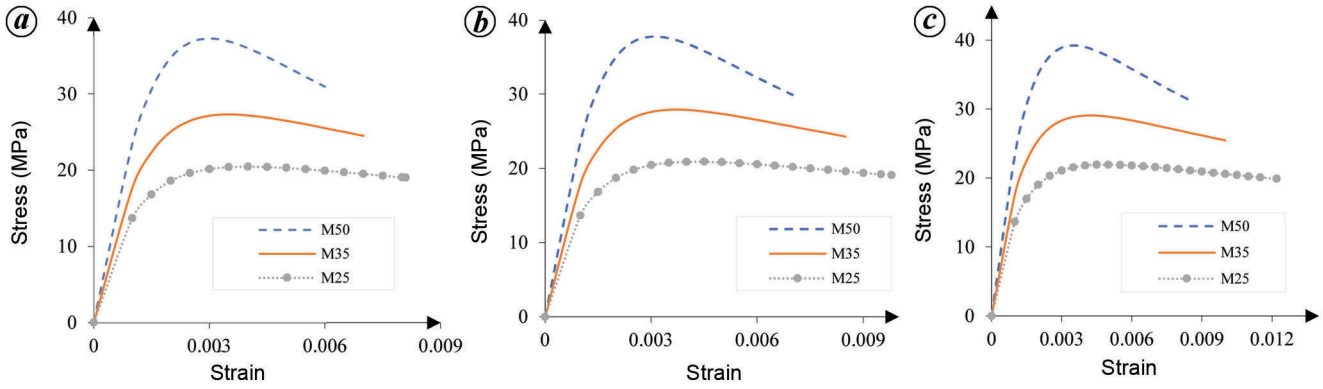

Figure 12. Stress–strain curve for confined concrete. ***a***, b_{eff} = 600 mm; ***b***, b_{eff} = 800 mml ***c***, b_{eff} = 1000 mm.

Table 4. Effect of the strength of concrete

		SCS				CCS			
		Unconfined		Confined		Unconfined		Confined	
Grade of concrete	b_{eff} (mm)	M_u (kN-m)	ϕ_u	M_u (kN-m)	ϕ_u	M_u (kN-m)	ϕ_u	M_u (kN-m)	ϕ_n
M25	600	600	0.017	647	0.042	708	0.019	758	0.044
	800	657	0.019	719	0.058	762	0.021	808	0.069
	1000	708	0.021	763	0.098	809	0.023	839	0.116
M35	600	668	0.019	713	0.039	772	0.021	805	0.046
	800	737	0.022	765	0.063	824	0.025	840	0.075
	1000	775	0.027	797	0.100	848	0.032	864	0.12
M50	600	753	0.023	760	0.045	832	0.027	838	0.054
	800	792	0.031	797	0.069	852	0.037	864	0.083
	1000	815	0.038	823	0.106	876	0.045	882	0.127

M_u is the ultimate moment; ϕ_u is the ultimate curvature.

is provided to M25-grade concrete. When the confinement is through an M50-grade concrete, improvement in M_u and φ_u is 10% and 20%, respectively (Table 4). M_u of CCS shows less improvement than SCS under confinement, but φ_u shows significant improvement. The impact of the effective flange width of concrete slab on M_u and φ_u of CCS and SCS is also noticeable. This demonstrates that increasing b_{eff} improves M_u and φ_u of the cross-section for both the confined and unconfined strength of concrete.

M–Φ relationship for different grades of concrete

For determining the effect of the grade of concrete on the *M–Φ* relationship of SCS and CCS, the parameters mentioned in Table 2 and their combinations were examined. Analysis results obtained from the program were expressed in terms of a non-dimensional plot, i.e. M_u/M_y and φ_u/φ_y (Figure 13 *a* and *b*). Besides, the analysis was performed for each slab width listed in Table 2, and the outcomes of composite sections with slab width of 1000 mm alone are presented here.

For SCS, M_u/M_y after attainment of yielding of the cross-section was always higher than CCS for the unconfined strength of concrete. CCS with M50-grade concrete resulted in a remarkable improvement in ϕ_u/ϕ_y after attaining yielding in cross-section compared with SCS. Considering the confined strength of concrete, M_u/M_y and ϕ_u/ϕ_y ratios after yielding the cross-section had improved for SCS and CCS (Figure 13 *b*). Confinement strength resulted in dynamic improvement of ϕ/ϕ_y in CCS when compared with SCS for a higher M50 grade of concrete.

Material utilization for different grades of concrete

The material utilization of the cross-section at the ultimate stage is influenced by the grade of concrete used for the composite beam. Figure 14 *a* shows the percentage of material used for beams having effective flange width of 1000 mm and unconfined concrete strength. Figure 14 *b* shows similar material utilization under confined concrete strength. In Figure 14 *a* and *b*, 'S' represent SCS, 'CL' represent CCS, 'st' is steel material, and 'c' is concrete material. Thus, for example, 'S-st' is the symbol used for representing the percentage utilization of steel material for SCS.

Figure 14 *a* shows that as the grade of concrete increases, the percentage of concrete utilization decreases, while the percentage of steel utilization increases. Achieving higher percentage utilization of steel material is preferable

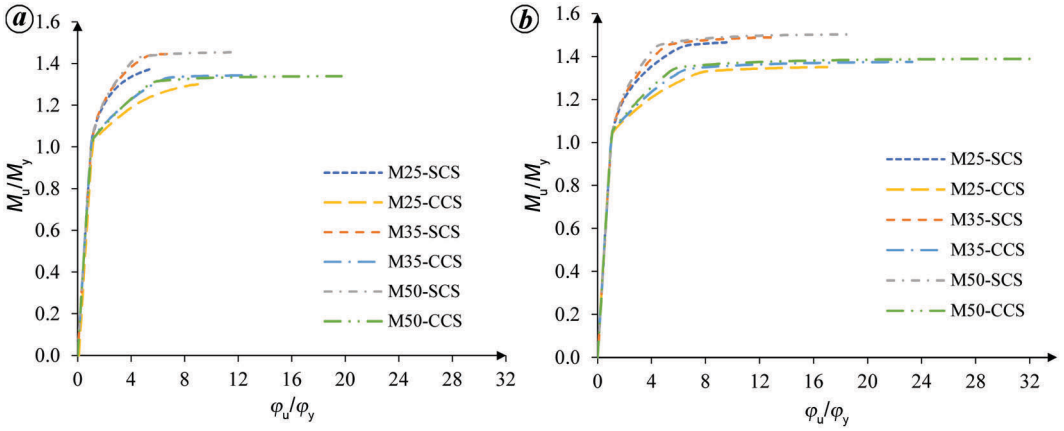

Figure 13. Effect of the grade of concrete on composite sections. (***a***) Unconfined and (***b***) confined strength of concrete.

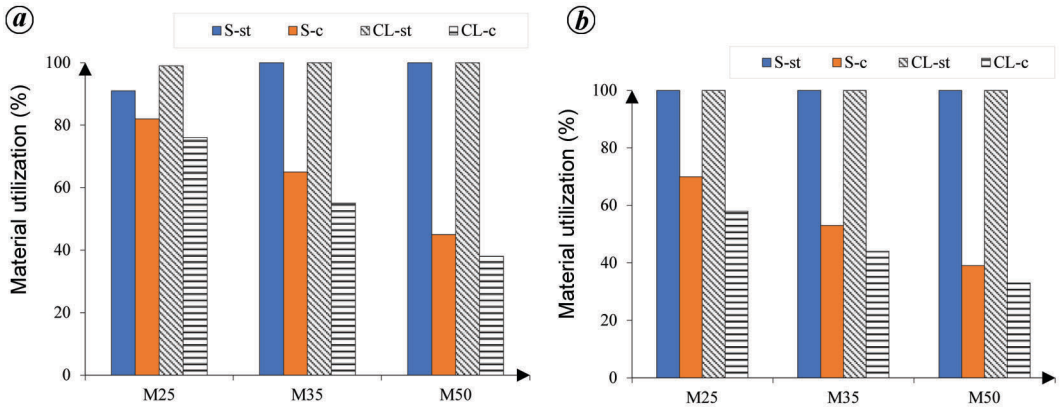

Figure 14. Effect of different grades of concrete on material utilization of the composite section with b_{eff} = 1000 mm. (***a***) Unconfined and (***b***) confined strength of concrete.

because of its higher cost, resulting in the required 'ductile failure' mode. The percentage utilization of concrete material was observed to be the least for the composite beam with a cellular steel section. The material utilization was significantly influenced by the effect of the confinement of concrete. Figure 14 *b* shows that the steel cross-section is 100% utilized for all the grades of concrete, while the utilization of concrete material keeps decreasing. This shows that the increased strength due to confinement provided to concrete results in a greater reduction of neutral axis depth (measured from the top fibre of the composite section) for a higher grade of concrete.

M–Φ relationship for different effective widths of the slab

Although all the concrete grades listed in Table 2 were considered, only the analysis results of composite sections with M25-grade concrete for various flange widths of the slab are presented here for comparison purposes. Figure 15 *a* and *b* shows the influence of b_{eff} on M_u/M_y and ϕ_u/ϕ_y ratios of the SCS and CCS cross-sections.

For SCS, the moment capacity ratio (M_u/M_y) after yielding the cross-section is always higher than that of CCS for all the considered b_{eff} values and concrete strength. CCS with a higher b_{eff} results in a remarkable improvement of curvature ratio (ϕ_u/ϕ_y) after yielding in cross-section compared with SCS for the respective effective flange width of the concrete slab. The availability of a higher b_{eff} and confinement results in a higher compressive force that concrete can bear before failure. Therefore, for higher b_{eff}, M_u/M_y and ϕ_u/ϕ_y after yielding the cross-section are improved for SCS and CCS respectively. Confinement to concrete results in drastic improvement of ϕ_u/ϕ_y of CCS when compared with SCS for higher b_{eff}.

Material utilization for different effective flange widths of the slab

Figure 16 *a* and *b* shows the percentage utilization of material for composite beams with unconfined and confined strength of concrete respectively. Moreover, these results are presented here for all considered composite beams having concrete of M25 grade with different b_{eff} values. From Figure 16 *a*, the percentage utilization of concrete (for S-c

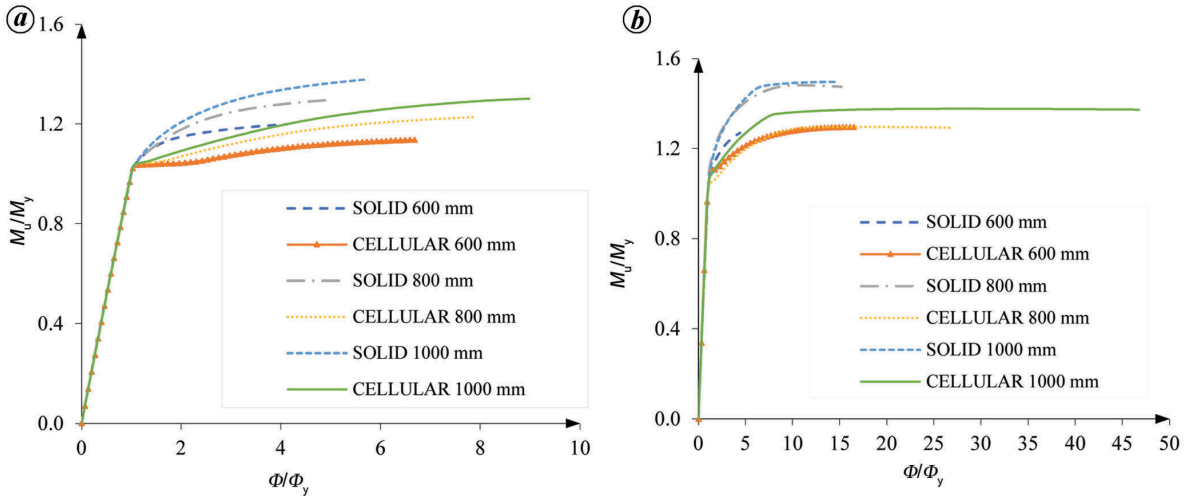

Figure 15. Effect of effective flange width of the slab on composite cross-sections. (***a***) Unconfined and (***b***) confined strength of concrete.

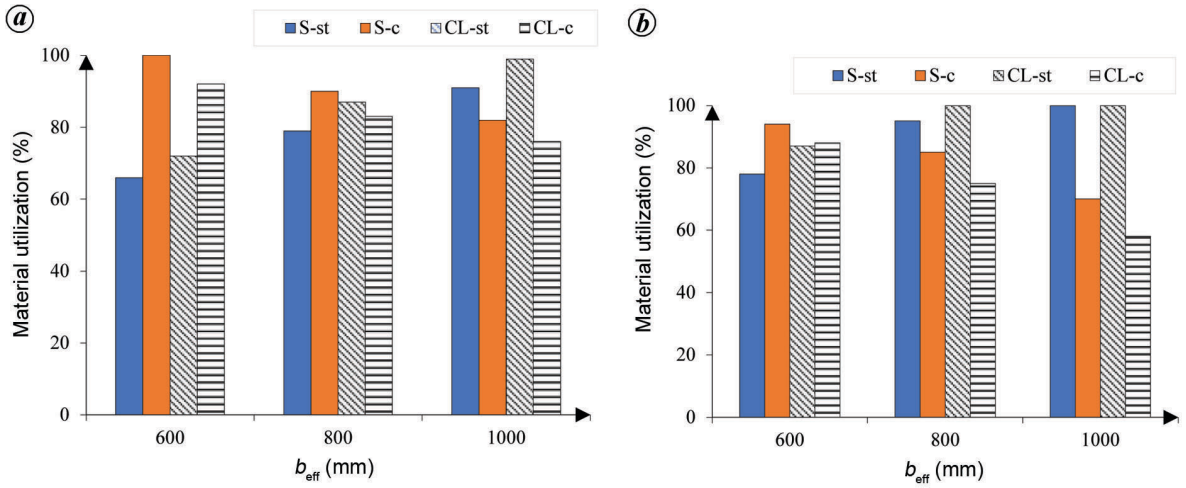

Figure 16. Effect of different b_{eff} values on material utilization of the cross-sections having M25-grade concrete. (***a***) Unconfined and (***b***) confined strength of concrete.

versus CL-c) is reduced, and for steel (for S-st versus CL-st), it is increased for higher b_{eff}. This results in the least percentage utilization of concrete material for CCS.

The higher b_{eff} value gives a high confined strength to the concrete. Figure 16 *b* shows that the steel cross-section is almost 100% utilized for only higher b_{eff}, while utilization of concrete material keeps reducing for confined strength of concrete. This effect is enhanced for CCS, and hence concrete utilization is minimum for a composite beam with a higher b_{eff} of a slab and cellular steel combination.

Conclusion

A strain compatibility based moment–curvature program for SCS and CCS has been developed and verified with FEM. The effect of cellularity and concrete confinement on the behaviour of solid and cellular composite beams was examined through parametric analysis. Based on the analysis results, the following conclusions are drawn.

- From the parametric study, it is observed that the behaviour of composite sections is enhanced under the effect of the confined strength of concrete and the use of cellular steel sections.
- In the case of unconfined SCS, increasing the slab's effective width (b_{eff}) helps improve the ultimate moment capacity (M_u) of composite sections. This impact is limited to certain higher grades of concrete. While in the case of ultimate curvature (ϕ_u), the impact of varying b_{eff} improves the ductile behaviour of composite sections.
- In the case of unconfined CCS, similar behaviour as shown by unconfined SCS is observed for ultimate moment capacity. However, compared to unconfined

SCS, an improvement in ϕ_u is seen as a result of increased effective slab width and escalating concrete grade.

- Concrete with confined strength impacts ϕ_u of SCS and CCS. For each considered increase in b_{eff} of confined CCS, a minimum of 1.5 times improvement in ϕ_u is obtained, while this improvement in the case of confined CCS is at least two times when compared with unconfined CCS.
- For CCS, the confinement given to concrete allows for the most efficient use of the steel material and results in higher curvature ductility before failure than with unconfined SCS.
- A higher grade of concrete and higher b_{eff}; whether unconfined or confined, result in better utilization of steel material for CCS than for SCS.

1. IS 11384, Code of practice for composite construction in structural steel and concrete. BIS, New Delhi, 2022.
2. EN 1994-1-1, Eurocode 4: design of composite steel and concrete structures – Part 1-1: general rules and rules for buildings. CEN, Brussels, Belgium, 2004.
3. Nethercot, D., *Composite Construction*, CRC Press, 2003.
4. Hauke, B., Economic application of composite beams with moderate high strength materials. In 5th European Conference on Steel and Composite Structures, Graz, Austria, 2008, pp. 3–5.
5. Nethercot, D. A., Composite steel and concrete structural members: fundamental behaviour. *Eng. Struct*., 1996, **18**(11), 886.
6. Shamass, R. and Cashell, K. A., Behaviour of composite beams made using high strength steel. *Structures*, 2017, **12**, 88–101.
7. Baskar, K. and Shanmugam, N. E., Steel–concrete composite plate girders subject to combined shear and bending. *J. Constr. Steel Res.*, 2003, **59**, 531–557.
8. Vasdravellis, G., Uy, B., Tan, E. L. and Kirkland, B., Behaviour and design of composite beams subjected to negative bending and compression. *J. Constr. Steel Res.*, 2012, **79**, 34–47.
9. Korkess, I. N., Yousifany, A. H., Abdul-Majeed, Q. and Husain, H. M., Behavior of composite steel–concrete beam subjected to negative bending. *Eng. Techonol.*, 2009, **27**, 53–72.
10. IS 800, General Construction in steel-code of practice. BIS, New Delhi, 2007.
11. Johnson, R. P., Composite structures of steel and concrete: beams, slabs, columns and frames for buildings. In *Composite Structures of Steel and Concrete*, John Wiley, 2018, pp. 1–265.
12. Kirkland, B., Kim, P., Uy, B. and Vasdravellis, G., Moment–shear–axial force interaction in composite beams. *J. Constr. Steel Res.*, 2015, **114**, 66–76.
13. Yakel, A. J. and Azizinamini, A., Improved moment strength prediction of composite steel plate girders in positive bending. *J. Bridge Eng.*, 2005, **10**, 28–38.
14. Zhao, H. and Yuan, Y., Experimental studies on composite beams with high-strength steel and concrete. *Steel Compo. Struct.*, 2010, **10**, 373–383.
15. Ismail, R. E. S., Fahmy, A. S. and Tawfik, N. M., Ultimate behavior of composite castellated beams under vertical loads. *Int. J. Comput. Appl.*, 2014, **108**, 40–46.
16. Al-Zuhairi, A. H. A., Mansi, A. I. and Anbar-Iraq, B., Behavior of composite concrete castellated steel beams in flexur. In 1st International Conference on Recent Trends of Engineering Sciences Sustainability, University of Baghdad – College of Engineering, 2017.
17. Ferreira, F. P. V., Martins, C. H. and de Nardin, S., Advances in composite beams with web openings and composite cellular beams. *J. Constr. Steel. Res.*, 2020, **172**, 106–182.
18. Popovics, S., A numerical approach to the complete stress–strain curve of concrete. *Cem. Concr. Res*., 1973, **3**, 583–599.
19. Mander, J. B., Priestley, M. J. N. and Park, R., Theoretical stress–strain model for confined concrete. *J. Struct. Eng.*, 1988, **114**, 1804–1826.
20. Renić, T. and Kišiček, T., Ductility of concrete beams reinforced with FRP rebars. *Buildings*, 2021, **11**.
21. Radnic, J., Markic, R., Harapin, A. and Matesan, D., Effect of confined concrete on compressive strength of RC beams. *Adv. Concr. Constr.*, 2013, **1**, 215–225.
22. Bing, L., Park, R. and Tanaka, H., Stress–strain behavior of high-strength concrete confined by ultra-high and normal-strength transverse reinforcements. *ACI Struct. J.*, 2001, **98**, 395–406.
23. Lokuge, W. P., Sanjayan, J. G. and Setunge, S., Stress–strain model for laterally confined concrete. *J. Mater. Civ. Eng.*, 2005, **17**, 607–616.
24. Jang, I.-Y., Park, H.-G., Kim, Y.-G., Kim, S.-S. and Kim, J.-H., Flexural behavior of high-strength concrete beams confined with stirrups in pure bending zone. *Int. J. Concr. Struct. Mater*, 2009, **3**, 39–45.
25. Djebli, B., Elddine, D. and Abidelah, A., Additional and total deflection of composite symmetric cellular beams. *J. Constr. Steel Res.*, 2019, **158**, 99–106.
26. Lawson, R. M., Lim, J., Hicks, S. J. and Simms, W. I., Design of composite asymmetric cellular beams and beams with large web openings. *J. Constr. Steel Res.*, 2006, **62**, 614–629.
27. Chung, K. F. and Lawson, R. M., Simplified design of composite beams with large web openings to Eurocode 4. *J. Constr. Steel Res.*, 2001, **57**, 135–164.
28. IS 12778, Hot rolled parallel flange steel sections for beams, columns and bearing piles – dimensions and section properties. BIS, New Delhi, 2004.
29. IS 456, Plain and reinforced concrete – code of practice. BIS, New Delhi, 2000.
30. IS 2062, Indian standard hot rolled medium and high tensile structural steel – Specification. BIS, New Delhi, 2011.

Received 12 October 2022; revised accepted 24 February 2023

doi: 10.18520/cs/v124/i12/1401-1411